

Development and Fabrication of Mesoporous Silica Loaded Nano-Gel of Ruallia Asperula Extract for Wound Healing

Shankar M. Dhobale^{a*}, Abhijeet A. Sonawane^b, Shailesh H. Hallale^{b*}, Mohan H. Shitole^c, Harshali N. Anap^c, Kuldeep H. Ramteke^d, Ravi D. Hole^e

^a Department of Pharmaceutics, SCSSS's Sitabai Thite College of Pharmacy, Shirur, Pune, 412210, Maharashtra, India.

^b Vishal Institute of Pharmaceutical Education and Research, Ale, Junnar, 412411, Pune, Maharashtra, India.

^c Department of Pharmaceutical Chemistry, SCSSS's Sitabai Thite College of Pharmacy, Shirur, Pune, 412210, Maharashtra, India

^d Department of Pharmaceutics, SCSSS's Sitabai Thite College of Pharmacy, Shirur, Pune, 412210, Maharashtra, India.

^e Department of Pharmaceutics, Samarth College of Pharmacy, Belhe Pune, Maharashtra, India.

^e Department of Pharmaceutics, Dattakala Shikshan Sanstha's, Dattakala Institute of Pharmaceutical Science and Research, Swami Chincholi, Daund, Pune, 413130, Maharashtra, India

Correspondences to Author:

Dr. Shankar M. Dhobale, Asso. Professor,

Email–drshankardhobale@gmail.com

Received: 16th Dec, 2025; Revised: 8th Feb 2026; Accepted: 12th Feb, 2026; Available Online: 28th Feb, 2026

ABSTRACT

Background: Ruallia asperula extract has strong wound-healing properties due to its anti-inflammatory, antimicrobial, and antioxidant effects. This study aimed to create and assess a mesoporous silica particle (MSP)-loaded nanogel that includes R. asperula extract to improve its therapeutic effect and stability.

Methods: We synthesized MSPs and characterized them for encapsulation efficiency, particle size, and thermal stability. We prepared a calibration curve for the extract and checked its solubility in different solvents. We formulated the nanogel using Carbopol 934p and PEG 400, optimizing it with a 3² factorial design. We evaluated the formulations for pH, spreadability, viscosity, and drug content, followed by in vitro release and stability studies.

Results: The calibration curve showed excellent linearity ($r^2 = 0.9996$). The extract had the highest solubility in ethanol (142.5 ± 12.64 mg/ml). MSPs showed a high encapsulation efficiency of $85.68 \pm 3.74\%$ with particle sizes of 173.4 ± 32.7 nm. The optimized nanogel (SF3) showed good physicochemical properties, achieving 90.04% drug release within 12 hours. Stability studies confirmed that the properties were maintained over three months.

Conclusion: The RA-MSP nanogel showed sustained release, stability, and promising potential for wound healing.

Keywords: Ruallia Asperula, mesoporous silica particles, nanogel, wound healing, encapsulation efficiency, in-vitro drug release, stability studies.

How to cite this article: Dhobale SM, Sonawane AA, Hallale SH, Shitole MH, Anap HN, Ramteke KH and Hole RD, Development and Fabrication of Mesoporous Silica Loaded Nano-Gel of Ruallia Asperula Extract for Wound Healing. Int J Drug Deliv Technol. 2026;16(20s): 161-175. DOI: 10.25258/ijddt.16.20s.19

Source of support: Nil.

Conflict of interest: None

1. INTRODUCTION

Wound healing is a complex and dynamic process that involves the coordinated efforts of various cellular, molecular, and biochemical events to restore the integrity of damaged tissue. This multifaceted process can be divided into four overlapping phases: haemostasis, inflammation, proliferation, and remodelling.[1] Each phase is critical and must occur in a precise sequence for successful healing. Haemostasis begins immediately after injury to prevent blood loss through clot formation. The inflammatory phase follows, characterized by the infiltration of immune cells that clear debris and pathogens from the wound site.[2] The proliferation phase involves the formation of new tissue, including the development of

new blood vessels (angiogenesis), synthesis of extracellular matrix (ECM), and re-epithelialization. Finally, the remodelling phase strengthens and reorganizes the ECM, leading to restored tissue function.[3] Despite advancements in wound care, chronic wounds remain a significant healthcare challenge, especially among the elderly and those with underlying conditions like diabetes.[4] The prevalence of chronic wounds is rising globally, contributing to substantial morbidity, prolonged hospital stays, and increased healthcare costs. Thus, developing effective wound healing therapies is of critical importance.[5]

Ruallia Asperula, a medicinal plant known for its therapeutic properties, has garnered attention for its

*Author for Correspondence: drshankardhobale@gmail.com

potential in wound healing applications.[6] This plant belongs to the Acanthaceae family and is traditionally used in various cultures for its anti-inflammatory, antimicrobial, and antioxidant properties.[7] The phytochemical analysis of *Ruallia Asperula* reveals a rich composition of bioactive compounds, including flavonoids, tannins, saponins, and glycosides. Flavonoids, in particular, are known for their ability to modulate oxidative stress and inflammation, two critical factors in the wound healing process. Tannins contribute to the astringent properties that can help in tissue contraction and wound closure. Additionally, saponins are recognized for their potential to enhance the permeability of cellular membranes, facilitating the delivery of active compounds to the wound site.[6] The diverse chemical constituents present in *Ruallia Asperula* make it a promising candidate for developing novel wound healing formulations, such as nano-gels, which can provide sustained and targeted delivery of these bioactives to enhance the healing process.[8]

Mesoporous silica particles (MSPs) have emerged as a versatile and promising material in the field of drug delivery and biomedical applications, particularly for wound healing.[9] These particles are characterized by their unique porous structure, which provides a high surface area and large pore volume, allowing for the efficient encapsulation and controlled release of therapeutic agents. The mesoporous nature of these particles facilitates the loading of various drugs, including small molecules, proteins, and herbal extracts, enabling a sustained and targeted delivery to the wound site. Additionally, MSPs exhibit excellent biocompatibility and stability, making them suitable for use in medical applications.[10] The ability to modify the surface properties of MSPs further enhances their functionality, allowing for the incorporation of bioactive molecules that can promote wound healing. By providing a conducive environment for cell proliferation and differentiation, MSPs can significantly enhance the wound healing process, reducing healing time and improving tissue regeneration.[10]

The objective of the current research is to develop and fabricate a mesoporous silica loaded herbal nano-gel containing *Ruallia Asperula* extract for enhanced wound healing. This study aims to harness the therapeutic potential of *Ruallia Asperula* in combination with the advanced delivery capabilities of MSPs to create an effective wound healing formulation. The specific objectives include the preparation and characterization of the mesoporous silica particles, the incorporation of *Ruallia Asperula* extract into the MSPs, and the formulation of the herbal nano-gel. By achieving these objectives, this research aims to provide a novel and efficient treatment modality for wound care, potentially addressing the limitations of current wound healing therapies and offering improved outcomes for patients with chronic and acute wounds.

2. MATERIALS AND METHODS

2.1. Materials

The *Ruallia Asperula* extract was obtained from Sciquaint Innovations (OPC) Private Limited in Pune, India (Ref No. SCI/analysis/2024/029). The supplier of Carbopol® 934P was Research Lab Fine Chem Industries, located in Mumbai, India. We bought the PEG 400, Triethanolamine, Methyl Paraben and Propyl Paraben from Pure Chemical India Pvt. Ltd. in Pune, India. All solvents and chemicals used were of the analytical grade.

2.2. Methods

2.2.1. Calibration Curve of *Ruallia Asperula* Extract

The calibration curve for *Ruallia Asperula* extract was established by scanning solutions of varying concentrations (from 10 to 60 ppm) within a range of 800 to 200 nm using the spectrum mode of a UV-Visible spectrophotometer. The absorbance maximum was identified during this scanning process. The absorbance of the solutions from 10 ppm to 60 ppm was measured using a Shimadzu double beam UV-spectrophotometer in photometric mode, with ethanol serving as a reference blank. The absorbance maxima were observed at 278 nm, providing the basis for the calibration curve.[11]

2.2.2. Synthesis of Mesoporous Silica Nanoparticles

A mixture comprising 48 grams of silica gel, 30 grams of sodium hydroxide, and an amount of sodium chloride to control the rate of polymerization was dissolved in 500 ml of distilled water. Sulfuric acid was added dropwise to this mixture at a rate of 200 ml/min until the pH reached approximately 7.0.[12] The resultant wet-gel slurry was thoroughly washed with distilled water to remove any residual salts. The washed slurry was then filtered using the Buchner method to obtain a wet cake, which was subsequently freeze-dried to yield the final mesoporous silica particles in their dry, fine form.[13]

2.2.3. Encapsulation of *Ruallia Asperula* Extract

A solution was prepared by mixing 10 ml of ethanol with 100 mg of *Ruallia Asperula* extract and then sonicated for 30 minutes in an ultrasonic water bath. After sonication, 500 mg of Mesoporous Silica Particles (MSPs) were thoroughly mixed with 100 mg of the *Ruallia Asperula* solution using a pestle and mortar. This mixture was then placed in an oven set at 50°C for 2 hours to evaporate the ethanol.[14] Once the ethanol had evaporated, 10 ml of distilled water was added to the dried mixture. Any unencapsulated *Ruallia Asperula* was separated by centrifugation at 5300 rpm for 10 minutes.[15]

2.2.4. Experimental Design

Nine different nano-gel formulations were formulated using a 3² factorial design, with the qualitative factors and levels detailed in Tables 1 and 2. The experimental design was generated and evaluated using Design Expert software (Expert® DX 13.0, StatEase Inc., MN). The study focused on two independent variables as amount of Carbopol® 934P (A) and the amount of PEG 400 (B). The dependent variables measured were spreadability (R1) and viscosity (cp) (R2).[16]

Table 1: Layout of Two Factor Three Level Design

Independent Variables						
Factors	Coded Values			Actual Values (%w/v)		
(A) Carbopol® 934P (%w/w)	-1	0	+1	0.5	1	1.5
(B) PEG 400 (%w/w)	-1	0	+1	1	1.5	2.5
Dependent Variables (Response)						
R1- Spreadability						
R2- Viscosity						

Table 2: RA-MSPs loaded gel compositions

Ingredients (%w/w)	SF1	SF2	SF3	SF4	SF5	SF6	SF7	SF8	SF9
RA loaded MSPs	0.5	0.5	0.5	0.5	0.5	0.5	0.5	0.5	0.5
Carbopol® 934P	0.5	1	1.5	0.5	1	1.5	0.5	1	1.5
PEG 400	1	1	1	1.5	1.5	1.5	2.5	2.5	2.5
Triethanolamine	0.5	0.1	0.1	0.1	0.1	0.1	0.1	0.1	0.1
Methyl Paraben	0.1	0.1	0.1	0.1	0.1	0.1	0.1	0.1	0.1
Propyl Paraben	0.02	0.02	0.02	0.02	0.02	0.02	0.02	0.02	0.02
Ethanol	1	1	1	1	1	1	1	1	1
Distilled water (q.s)	100	100	100	100	100	100	100	100	100

2.2.5. Preparation of RA-MSPs loaded gel.

The RA-MSPs loaded gel was prepared by first dispersing the Mesoporous Silica Particles (RA-MSPs) in distilled water to create a base. Carbopol 934p was then added as a gelling agent, with continuous stirring to ensure uniform distribution and prevent clumping.[17] PEG 400 was incorporated to enhance the viscosity of the gel, and thorough mixing was performed to achieve homogeneity. Triethanolamine was added in controlled amounts to adjust the pH of the gel, with careful stirring to reach the desired level. Methyl Paraben was included as a preservative to extend the gel's shelf life. The volume and consistency of the gel were adjusted by adding distilled water as needed.[18] Finally, the mixture was left to rest, allowing the formation of a stable and uniform gel matrix that effectively encapsulated the RA-MSPs, ensuring a smooth and homogeneous final product.

2.2.6. Characterization of Mesoporous silica particles

2.2.6.1. Zeta potential and particle size analysis

The particle size of every sample was determined using dynamic light scattering. The zeta potential was calculated or measured using the electrophoretic mobility beneath the electrical field as the average value of the three measurements, and the average of at least three measurements was recorded.[19]

2.2.6.2. % Entrapment efficiency

The samples were subjected to UV visible spectroscopy (UV-1800, Shimadzu) at 278 nm after being diluted with ethanol at a ratio of 1:8 (v/v). As previously noted, a reference experiment was conducted, but instead of dissolving the RA-MSP mixture in ethanol, the absorbance was measured at 278 nm.[20]

$$\text{Loading Efficiency} = \frac{W_{total} - W_{free}}{W_{total}} \times 100 \quad (1)$$

Where, W is weight of fraction in mg.

2.2.7. Evaluation of RA-MSPs loaded gel. a comprehensive assessment of its appearance, colour, Odor, and solubility. The appearance was carefully inspected for consistency and uniformity, ensuring that it met the visual standards. The color was evaluated against a standardized colour chart to confirm its appropriateness. The odor was examined to ensure it was within acceptable limits and free from any unusual or off-putting smells. Lastly, the solubility of the drug product was tested in various solvents to verify that it met the required solubility standards, ensuring its effectiveness and stability.[21]

2.2.7.2. FTIR Analysis

Fourier-transform infrared (FTIR) spectroscopy was used to assess the drug-excipient compatibility. The physical mixture of excipients (RA-MSPs loaded gel) and *Ruallia Asperula* extract were dried at 50°C. After being combined with KBr, the dry samples were compacted into pellets. A Perkin Elmer Spectrum 100 FTIR spectrophotometer was used to record the FTIR spectra of the physical mixture of excipients (RA-MSPs loaded gel) and the pure *Ruallia Asperula* extract. The characteristic peaks of the medicine and excipients were examined in the spectra for any shifts or changes that might suggest a possible interaction between them.[22]

2.2.7.3. Differential Scanning Calorimetry (DSC) Studies

The thermal behaviour of *Ruallia Asperula* extract and its compatibility with the excipients utilized in the RA-MSPs loaded gel formulation were investigated using differential scanning calorimetry (DSC) tests. In a DSC equipment (Perkin Elmer DSC-8000), *Ruallia Asperula* extract and the physical mixture of excipients (RA-MSPs loaded gel) were separately weighed and heated at a rate of 10°C/min from 30°C to 250°C. The physical mixture of excipients (RA-MSPs loaded gel) and pure *Ruallia Asperula* extract

*Author for Correspondence: drshankardhobale@gmail.com

thermal curves were recorded and examined for any shifts or modifications in the distinctive peaks, indicating any interactions between the medication and excipients. The outcomes were utilized to assess how well the medication worked with the excipients in the RA-MSPs loaded gel formulation.[22]

2.2.7.4. pH Determination

A digital pH meter (ELICO LI 613) was used to measure the pH of the produced gel. After dissolving 1 gram of gel in 100 millilitres of distilled water, the mixture was left for two hours. The glass electrode was then dipped into the gel. Each formulation's pH was measured three times, and the average results were determined.[23]

2.2.7.5. Spreadability

A modified slide method was used to assess the spreadability of the gel formulations loaded with RA-MSPs. One glass slide had a little amount of gel loaded with RA-MSPs, and another slide was positioned on top of it. A Vernier Caliper was used to measure the diameter of the distributed RA-MSPs laden gel in both directions after the top slide was lifted after a 1 kg weight was applied to it for 5 minutes.[23] The formula below was used to determine the spreadability:

$$S = M.L/T$$

Where,

M= weight tied to upper slide (10g)

L = length of glass slide (6.8cm)

T = Time taken to separate the slides

3. RESULTS AND DISCUSSION

3.1. Calibration curve of *Ruallia Asperula* extract

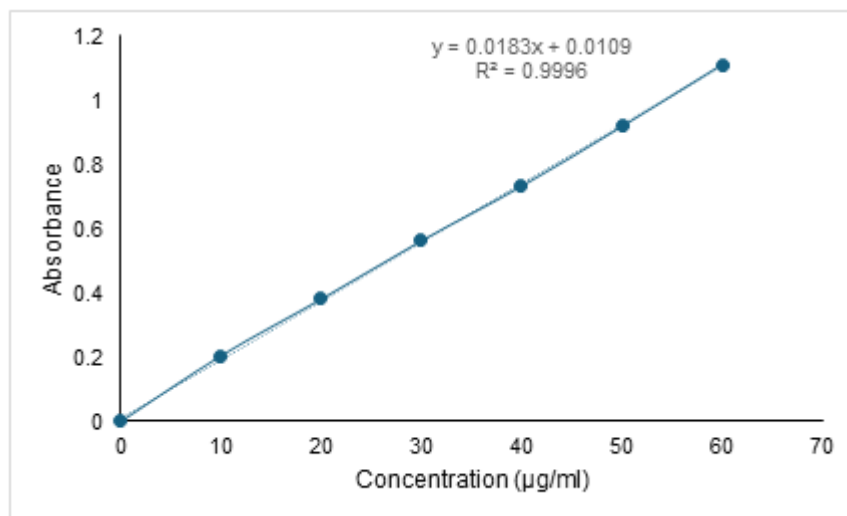


Figure 1: Calibration curve of *Ruallia Asperula* extract in ethanol

2.2.7.6. Viscosity

The viscosities of nine freshly produced formulations were initially determined using a Brookfield viscometer with spindle number 4. Rotating at a speed of 2.5 rpm for 5 minutes, the spindle was carefully dropped perpendicularly into the middle of the gel formulation in a beaker, ensuring that it did not contact the bottom of the beaker. The measured viscosity was recorded.[24]

2.2.7.7. In-vitro drug release studies

The gel formulation's in vitro release was studied using a Franz diffusion cell, which has two chambers: the giver and receptor compartments. The receptor compartment had a testing port, and the provider compartment, which was open at the top and exposed to air, was kept at a temperature of $37 \pm 0.5^\circ\text{C}$. The dispersion media was phosphate buffer (pH 7.4). A magnetic bead was used to constantly agitate the fluid while the entire assembly was held on a magnetic stirrer. As a control, a comparable blank set was run concurrently. At appropriate times, the sample (5 ml) was removed and replaced with the same volume of brand-new dissolving media. Using spectrophotometric analysis at 278 nm, samples were determined to determine the cumulative percentage of drug release. In each case, the real reading was determined by comparing the drug release and control readings.[24]

2.2.7.10. Statistical Analysis

Design Expert® DX 13.0 (StatEase Inc., MN) was used to evaluate the experiment data. Response surface plots were used to display the factors' impacts on the dependent variables after analysis of variance (ANOVA) was used to assess the factors' significance.

RESEARCH PAPER

The calibration curve constructed from these absorbance values further substantiates the linear relationship between concentration and absorbance, with a slope of 0.0183 and an intercept of 0.0109 (Figure 1). The high correlation coefficient ($r^2 = 0.9996$) underscores the precision and reliability of the absorbance measurements, validating the method's suitability for quantitative analysis of *Ruallia*

Asperula in ethanol. This robust calibration curve is essential for accurately determining the concentration of unknown samples in future analyses, ensuring the reproducibility and accuracy of the experimental results. The thorough investigation of absorbance maxima and the subsequent calibration curve provide a solid foundation for further analytical studies involving *Ruallia Asperula*.

3.2. Solubility Analysis

Table 3: Results of solubility analysis of *Ruallia Asperula* Extract

Sr. No.	Solvent	Solubility (mg/ml)	Results
1	Water	0.7±0.04	Very Slightly soluble
2	Ethanol	142.5±12.64	Freely soluble
3	Chloroform	57.8±8.54	Soluble
4	Phosphate Buffer pH 6.8	33.65±0.32	Soluble

Data are expressed in mean±SD (n = 3)

The solubility analysis of *Ruallia Asperula* extract (Table 3) reveals significant

2.2.7.1. Morphological Evaluation

The morphological evaluation of the drug product involved variability across different solvents. The extract is very slightly soluble in water, with a solubility of 0.7±0.04 mg/ml, indicating limited aqueous solubility. In contrast, the extract is freely soluble in ethanol, demonstrating a high solubility of 142.5±12.64 mg/ml. It is also soluble in chloroform and phosphate buffer pH 6.8, with solubility values of 57.8±8.54 mg/ml and 33.65±0.32 mg/ml, respectively. These results highlight ethanol as the most effective solvent for dissolving *Ruallia Asperula* extract, while also confirming the extract's moderate solubility in chloroform and phosphate buffer pH 6.8, which are suitable for various formulation applications.

3.3. Results of Fourier transform infrared (FTIR) spectroscopy

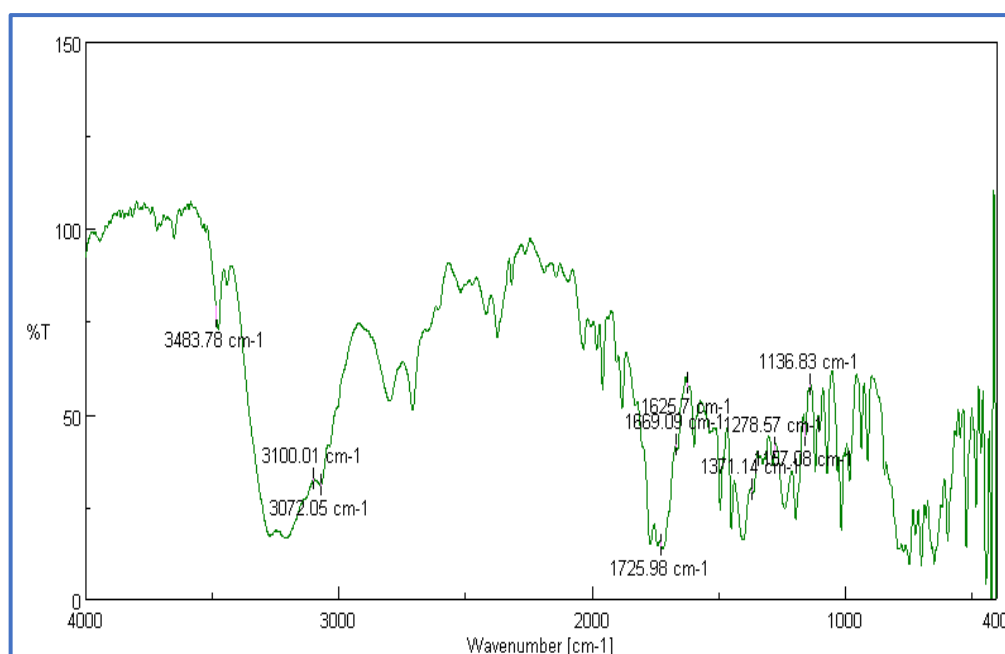


Figure 2: FT-IR spectra of Extract (*Ruallia Asperula*)

*Author for Correspondence: drshankardhobale@gmail.com

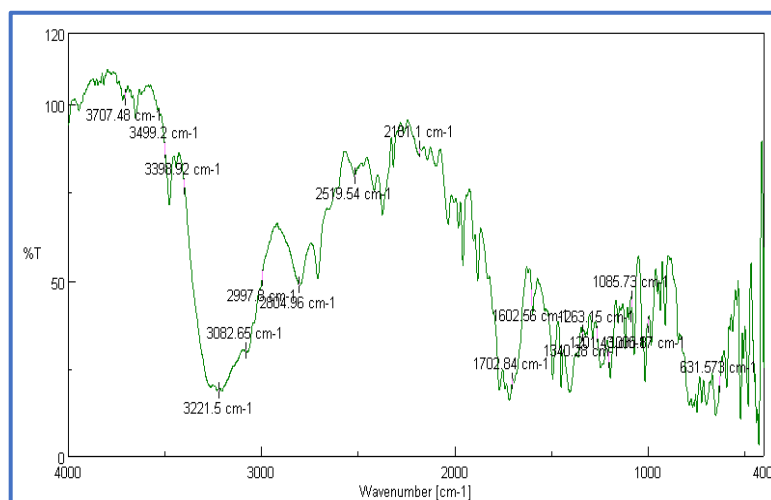


Figure 3: FT-IR spectra of *Ruallia Asperula* Extract + Excipients

The FTIR analysis of the *Ruallia Asperula* (R.A.) pure extract and the *Ruallia Asperula* Extract + Excipients reveals that the primary functional groups of the drug remain intact when incorporated into the nanogel formulation. This is indicative of a positive outcome, demonstrating that there are no significant chemical interactions between the drug and the excipients. The Figure 2 and 3 the hydroxyl (O-H) stretch shows a slight shift from 3483.78 cm^{-1} in the pure extract to 3499.2 cm^{-1} in the nanogel. Similarly, the amine (N-H) stretches shifts from 3100.01 cm^{-1} to 3221.5 cm^{-1} , and the aromatic C-H stretch from 3072.05 cm^{-1} to 3082.65 cm^{-1} . These minor shifts suggest potential hydrogen bonding or weak interactions but do not indicate any significant chemical modification of the drug. The carbonyl (C=O) stretches peaks at 1669.09 cm^{-1} and 1725.98 cm^{-1} in the pure extract show slight shifts to 1702.84 cm^{-1} in the nanogel, which again indicates preservation of the carbonyl groups

with minor interactions. The C=C (alkene) and C-H (methylene) stretches exhibit minimal shifts, from 1625.7 cm^{-1} to 1602.56 cm^{-1} and from 1371.14 cm^{-1} to 1340.28 cm^{-1} respectively. The presence of new peaks in the nanogel spectrum, such as the O-H out-of-plane bend at 3707.48 cm^{-1} and 3398.92 cm^{-1} , and the alkyne (C≡C) stretch at 2181.1 cm^{-1} , can be attributed to the excipients used in the formulation. These new peaks do not overlap or interfere with the characteristic peaks of *Ruallia Asperula*, further confirming the absence of adverse interactions. The FTIR spectra analysis confirms that the key functional groups of *Ruallia Asperula* are preserved when mixed with Excipients, with only minor shifts indicating weak interactions rather than significant chemical alterations. This compatibility between the drug and the excipients suggests that the *Ruallia Asperula* Extract + Excipients is a stable and suitable formulation for *Ruallia Asperula*, ensuring its efficacy and safety

3.4. Results of Differential scanning calorimetry (DSC) studies

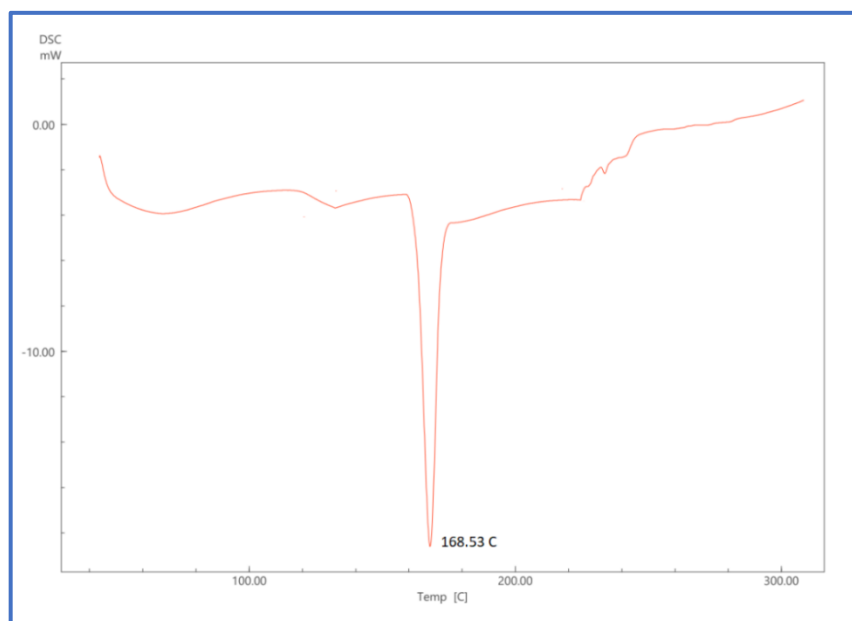


Figure 4: DSC of *Ruallia Asperula* Extract

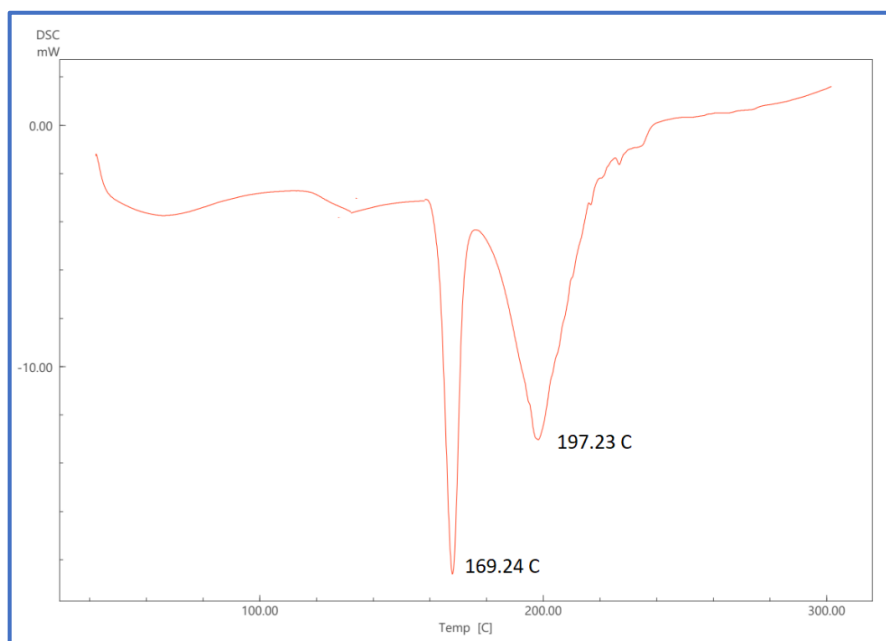


Figure 5: DSC of *Ruallia Asperula* Extract + Excipients

The Differential Scanning Calorimetry (DSC) analysis provides critical insights into the thermal behaviour and compatibility of *Ruallia Asperula* (R.A.) when incorporated into the MSPs loaded nanogel. The DSC thermogram of the pure *Ruallia Asperula* extract, as shown in Figure 4, exhibits a distinct endothermic peak at 168.53°C, which corresponds to the melting point of the pure drug. This peak is indicative of the crystalline nature of *Ruallia Asperula* in its unformulated state. In the DSC thermogram of the *Ruallia Asperula* Extract + Excipients (Figure 5), the presence of two endothermic peaks at 169.24°C and 197.23°C was observed. The peak at 169.24°C is very close to the melting point of the pure drug, suggesting that *Ruallia Asperula* retains its crystalline structure within the nanogel formulation. The slight shift to a higher temperature indicates a minor

interaction between the drug and the excipients, potentially due to the encapsulation process. The additional peak at 197.23°C can be attributed to the excipients or the formation of a new phase due to the interaction between the drug and the MSPs matrix. However, this new peak does not overlap or significantly alter the melting point of *Ruallia Asperula*, demonstrating that the drug's thermal stability is maintained. The DSC analysis confirms that the thermal properties of *Ruallia Asperula* are largely preserved in the *Ruallia Asperula* Extract + Excipients, with only minor shifts. This stability is crucial for ensuring that the drug maintains its efficacy and integrity during formulation and storage, highlighting the suitability of *Ruallia Asperula* Extract + Excipients as a delivery system for *Ruallia Asperula*.

3.5. Characterization of R.A. Loaded MSPs

3.5.1. Entrapment efficiency

Table 4: Results of % Entrapment efficiency

Sr. No.	Formulation	% Entrapment efficiency
1	R.A. Loaded MSPs	85.68 ± 3.74%

Data are expressed in mean±SD (n = 3)

The results of the entrapment efficiency analysis are presented in Table 4, revealing that the R.A. loaded MSPs achieved an entrapment efficiency of 85.68 ± 3.74%. This high entrapment efficiency suggests that the formulation method is effective, ensuring that a significant portion of *Ruallia Asperula* is encapsulated within the MSPs. The relatively low standard deviation indicates consistent and

reproducible encapsulation, which is crucial for the reliability of the drug delivery system. High entrapment efficiency is essential for maximizing the therapeutic potential of *Ruallia Asperula*, reducing wastage, and ensuring a controlled release profile. This characterization confirms the suitability of MSPs as a delivery vehicle for *Ruallia Asperula*, potentially enhancing its clinical efficacy.

3.5.2. Result of Particle Size Analysis

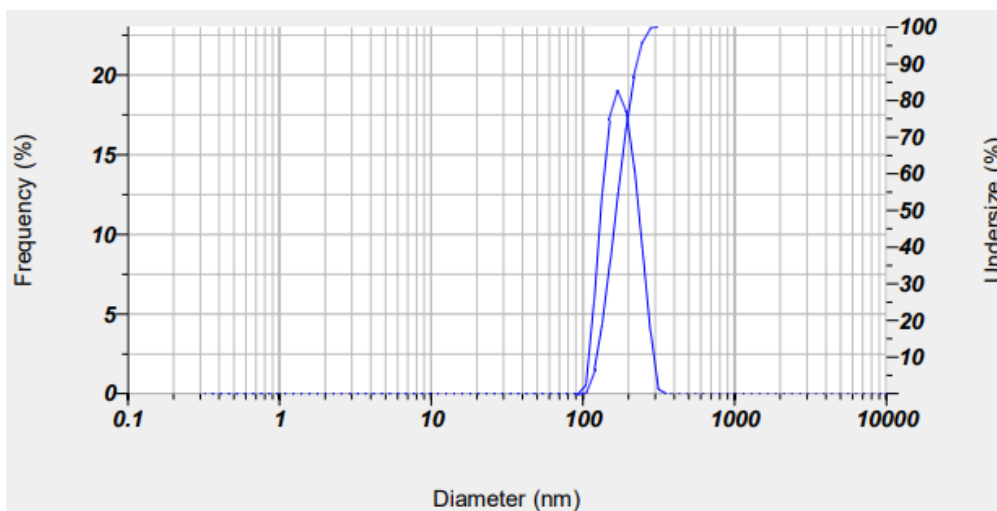


Figure 6: Particle size analysis of the R.A. loaded MSPs.

Table 5: Particle Size Analysis of MSPs

Sr. No.	Formulation	Particle size (nm)
1	R.A. Loaded MSPs	173.4 ± 32.7

Values are expressed in mean±SD (n = 3)

The particle size of the R.A. loaded MSPs as shown in Table 5 was measured at 173.4 ± 32.7 nm. This indicates a relatively narrow size distribution, which is advantageous for ensuring consistent drug delivery and absorption. The nanoscale size of the particles is particularly beneficial for enhancing the solubility and bioavailability of *Ruallia*

Asperula, facilitating its passage through biological membranes and promoting efficient uptake by target cells. The low standard deviation reflects uniformity in particle size, which is essential for predictable and reproducible drug release profiles. Overall, the particle size analysis confirms that the R.A. loaded MSPs are suitably sized for potential pharmaceutical applications, enhancing the therapeutic prospects of *Ruallia Asperula*.

3.6. Evaluations of RA-MSPs loaded Nanogel.

Table 6: Physical evaluation of Nanogel formulations

Batch	Colour	Appearance	Odor
SF1	Greenish Brown	Clear, Thick	Odourless
SF2	Greenish Brown	Clear, Thick	Odourless
SF3	Greenish Brown	Clear, Thick	Odourless
SF4	Greenish Brown	Clear, Thick	Odourless
SF5	Greenish Brown	Clear, Thick	Odourless
SF6	Greenish Brown	Clear, Thick	Odourless
SF7	Greenish Brown	Clear, Thick	Odourless
SF8	Greenish Brown	Clear, Thick	Odourless
SF9	Greenish Brown	Clear, Thick	Odourless

Table 7: pH, Determination, spreadability, and viscosity results for formulated batches.

Batch	pH	Spreadability (gm/cm.sec)	Viscosity (cps)	Drug Content (% w/w)
SF1	6.69±0.05	11.8±0.05	15925±254.61	87.43±0.72
SF2	6.63±0.02	12.9±0.07	17768±291.45	89.25±0.61
SF3	6.54±0.04	13.6±0.05	17727±199.84	91.07±0.54
SF4	6.87±0.03	8.3±0.06	9865±142.12	88.32±0.67
SF5	6.78±0.02	9.7±0.05	11632±132.67	90.11±0.59
SF6	6.69±0.03	11.1±0.05	12923±145.88	92.04±0.51
SF7	7.01±0.02	5.4±0.04	12478±166.41	89.66±0.64
SF8	6.92±0.03	6.7±0.07	13576±156.93	91.52±0.57
SF9	6.82±0.04	8.1±0.06	12986±165.87	93.41±0.49

Values are expressed in mean±SD (n=3)

The physical evaluation of the MSPs loaded nanogel formulations (Table 6) reveals consistent characteristics

across all batches (SF1-SF9). All batches exhibit a greenish-brown colour, attributed to the inherent colour of the *Ruallia Asperula* extract. The gels are described as

clear and thick, indicating a uniform and homogenous consistency without visible signs of phase separation or precipitation. Additionally, all batches are odourless, suggesting the absence of volatile compounds or degradation products that could affect the formulation's stability and acceptability. These uniform physical attributes across all batches suggest that the manufacturing process is robust and reproducible.

The results of pH determination, spreadability, and viscosity for all batches are detailed in Table 7, along with the drug content. The pH values of the formulations range from 6.54 to 7.01, which is within the acceptable range for topical formulations, ensuring skin compatibility and minimizing the risk of irritation. Spreadability, measured in gm/cm.sec, varies from 5.4 to 13.6 across the batches, indicating differences in the ease of application, with higher values such as 13.6 for SF3 suggesting easier application over larger surface areas. Viscosity measurements, ranging from 9865 to 17768 cps, indicate the thickness and flow characteristics of the gels, with higher viscosity in batches like SF2 and SF3 potentially providing more sustained drug release, while lower viscosity batches like SF4 might offer quicker absorption. Drug content analysis reveals high and consistent drug loading, ranging from 87.43% to 93.41%, indicating efficient encapsulation and minimal drug loss. These evaluations demonstrate consistent physical characteristics, appropriate pH levels for skin application, varying spreadability and viscosity for different application needs, and high drug content across all batches, highlighting the successful formulation of the nanogels and the optimization of the manufacturing process for large-scale production.

3.7. Optimization of the Concentrations of Carbopol 934 and PEG 400 using 3² Full Factorial design.

3.7.1. Effect of formulation variables on Spreadability (R1)

$$\text{Spreadability (R1)} = +8.60 + 1.24A - 3.02B + 0.1875AB - 0.0500A^2 + 0.19B^2 \dots \dots \dots (1)$$

The optimization of the MSPs loaded nanogel formulation was conducted using a quadratic model to evaluate the effect of two critical variables: Carbopol® 934P (A) and PEG 400 (B) concentrations, on the spreadability (R1) of the gel. The ANOVA results for the quadratic model are detailed in Table 8 and highlight the significance and contribution of each factor and their interactions. The model's sum of squares, mean square, F-value, and p-value indicate a highly significant relationship between the model and the spreadability response, with a p-value of 0.0005, confirming the model's reliability. The individual effects of Carbopol® 934P and PEG 400 are also significant, with p-values of 0.0012 and < 0.0001, respectively. This demonstrates that both components significantly influence the spreadability of the nanogel. The interaction term (AB) and the quadratic term for Carbopol® 934P (A²) were not significant, suggesting minimal interaction effects and non-linearity for Carbopol® 934P within the studied range. However, the quadratic term for PEG 400 (B²) was significant (p =

0.0094), indicating a non-linear effect of PEG 400 on spreadability.

The model's standard deviation is 0.2455, and the coefficient of determination (R²) is 0.9972, indicating that 99.72% of the variability in spreadability can be explained by the model. The adjusted R² value of 0.9924 further supports the model's goodness of fit, accounting for the number of predictors in the model. The coefficient of variation (C.V. %) of 2.52% signifies low variability relative to the mean spreadability value, reflecting high precision and reliability of the experimental data. The predicted R² of 0.9683 indicates that the model has strong predictive capabilities, as it closely matches the adjusted R². The Adeq Precision value of 42.4435, which measures the signal-to-noise ratio, is well above the desired threshold of 4, indicating an adequate signal. The ANOVA and fit statistics validate that the quadratic model effectively captures the influence of Carbopol® 934P and PEG 400 on the spreadability of the MSPs loaded nanogel, guiding the optimization process to achieve desirable formulation characteristics.

Figure 7a presents the contour plot for Spreadability (R1), which visually represents the relationship between Carbopol® 934P (A) and PEG 400 (B) concentrations. The contour lines illustrate how variations in the concentrations of these two components influence the spreadability of the MSPs loaded nanogel. The plot demonstrates that an increase in Carbopol® 934P generally improves spreadability up to a certain point, as indicated by the upward trend in the contour lines. Conversely, increasing PEG 400 initially decreases spreadability, as seen by the downward trend. The interaction between Carbopol® 934P and PEG 400 is minimal, with contour lines showing almost parallel trends, indicating that their combined effect is primarily additive rather than synergistic or antagonistic. This visual representation helps identify the optimal concentration ranges for both excipients to achieve the desired

Figure 7b provides a 3D response surface plot for Spreadability (R1), offering a three-dimensional view of the relationship between the independent variables (Carbopol® 934P and PEG 400) and the dependent variable (spreadability). The plot clearly shows a peak, indicating the optimal region where the spreadability is maximized. The surface plot corroborates the findings from the contour plot, illustrating that higher levels of Carbopol® 934P enhance spreadability, whereas higher levels of PEG 400 have a diminishing effect. The curvature of the surface confirms the significant quadratic effect of PEG 400 on spreadability, as identified in the ANOVA results. This 3D visualization aids in understanding the complex interactions and helps in pinpointing the exact formulation conditions for optimal spreadability.

3.7.2. Effect of formulation variables on Viscosity (R2)

$$\text{Viscosity (R2)} = +10698.94 + 848.68A - 2063.33B + 413.$$

$$+4827.50B^2 \dots \dots \dots$$

This equation (1) illustrates that while increasing Carbopol® 934P concentration generally increases viscosity, increasing PEG 400 concentration decreases it. The significant quadratic term for PEG 400 indicates a

strong non-linear relationship, where the viscosity decreases sharply with increasing PEG 400 concentration. The ANOVA results for the quadratic model assessing the viscosity (R₂) of the MSPs loaded nanogel formulations (Table 8) indicate significant

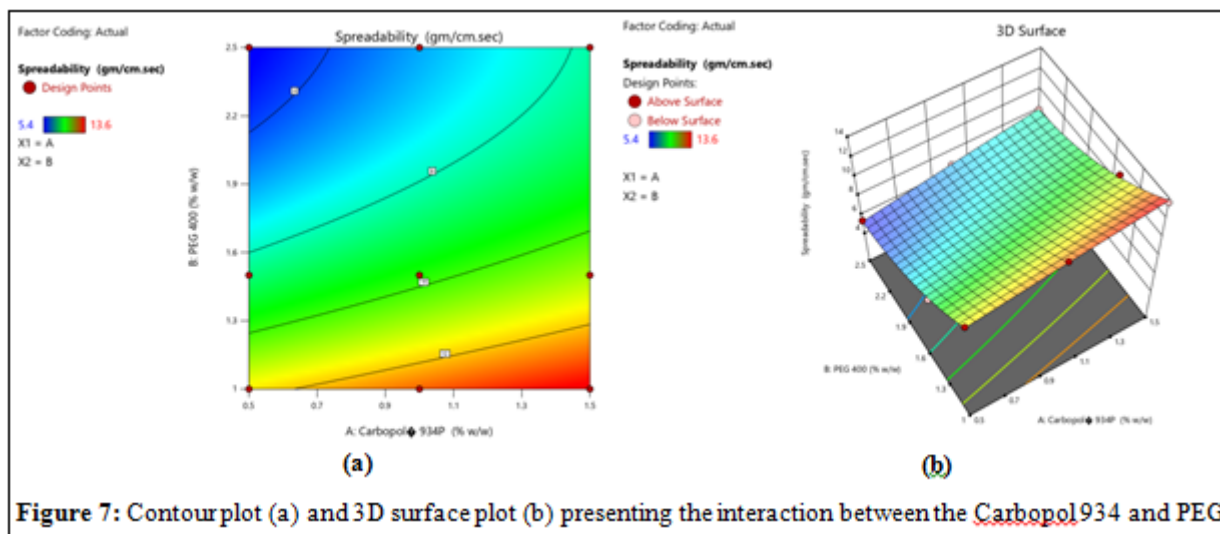


Figure 7: Contour plot (a) and 3D surface plot (b) presenting the interaction between the Carbopol934 and PEG

effects of the independent variables, Carbopol® 934P (A) and PEG 400 (B). The model's sum of squares and mean square values demonstrate a high degree of variability explained by the model, with an F-value of 31.34 and a p-value of 0.0086, indicating the model's overall significance. The individual contributions of Carbopol® 934P and PEG 400 are also significant, with p-values of 0.0428 and 0.0036, respectively. These results highlight that both components significantly influence the viscosity of the nanogel. However, the interaction term (AB) and the quadratic term for Carbopol® 934P (A²) are not significant, with p-values of 0.2597 and 0.2146, respectively, indicating minimal interaction effects and non-linearity for Carbopol® 934P. The quadratic term for PEG 400 (B²) is highly significant (p = 0.0023), suggesting a pronounced non-linear effect of PEG 400 on viscosity.

The models show standard deviation as 608.01, and the coefficient of determination (R²) is 0.9812, indicating that 98.12% of the variability in viscosity is explained by the model. The adjusted R² value of 0.9499 supports the model's goodness of fit, accounting for the number of predictors. The coefficient of variation (C.V. %) of 4.38% indicates low variability relative to the mean viscosity, reflecting high precision. The predicted R² of 0.8026, although slightly lower than the adjusted R², still indicates good predictive capabilities. The Adeq Precision value of 15.9454, which measures the signal-to-noise ratio, is well above the threshold of 4, indicating an adequate signal. The ANOVA results and fit statistics validate the quadratic model for viscosity, confirming that Carbopol® 934P and PEG 400 significantly influence the viscosity of the MSPs loaded nanogel. These findings provide valuable insights into the formulation optimization, ensuring the desired

viscosity characteristics are achieved for enhanced performance and stability of the final product.

Figure 8a presents the contour plot for Viscosity (R₂), illustrating the relationship between Carbopol® 934P (A) and PEG 400 (B) concentrations. The contour lines show how changes in the concentrations of these two components affect the viscosity of the MSPs loaded nanogel. The plot reveals that increasing the concentration of Carbopol® 934P generally leads to higher viscosity, as indicated by the upward trend in the contour lines. Conversely, increasing the concentration of PEG 400 results in a decrease in viscosity, shown by the downward trend. The nearly parallel contour lines suggest minimal interaction between Carbopol® 934P and PEG 400, implying that their effects on viscosity are largely independent. This visual representation helps in identifying the optimal concentration ranges for both excipients to achieve the desired viscosity.

Figure 8b provides a 3D response surface plot for Viscosity (R₂), offering a three-dimensional perspective on how Carbopol® 934P and PEG 400 concentrations influence the viscosity. The plot clearly shows a peak, indicating the region where the viscosity is maximized. The 3D surface plot corroborates the findings from the contour plot, demonstrating that higher concentrations of Carbopol® 934P enhance viscosity, while higher concentrations of PEG 400 reduce it. The curvature of the surface plot further confirms the significant quadratic effect of PEG 400 on viscosity, as identified in the ANOVA results. This 3D visualization helps in understanding the complex interactions and provides a clearer picture of the formulation conditions required for optimal viscosity.

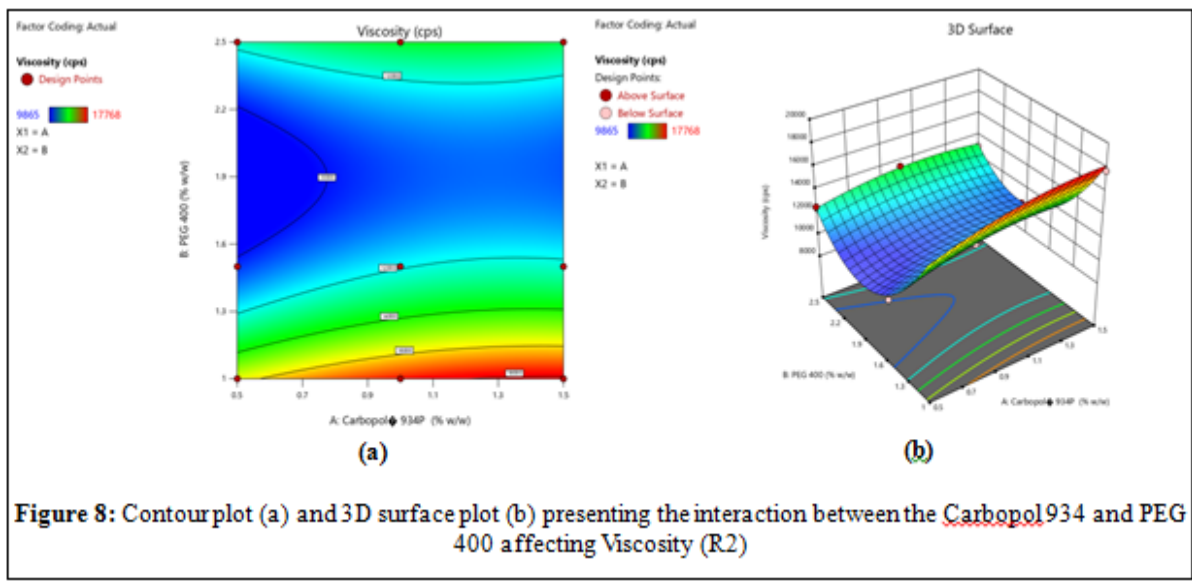


Figure 8: Contourplot (a) and 3D surface plot (b) presenting the interaction between the Carbopol934 and PEG 400 affecting Viscosity (R2)

3.8. Results of regression analysis

Table 8: ANOVA results for the quadratic model for the response Spreadability (R1) and Viscosity (R2).

Response	Result value
Spreadability (R1)	
Sum of squares	63.64
Df	5
Mean square	12.73
F Value	211.15
P value	0.0005
R ²	0.9972
Adjusted R ²	0.9924
Predicted R ²	0.9683
Std. Dev.	0.2455
Mean	9.73
C.V. %	2.52
Significant	
Viscosity (R2)	
Sum of squares	5.794
Df	5
Mean square	1.159
F Value	31.34
P value	0.0086
R ²	0.9812
Adjusted R ²	0.9499
Predicted R ²	0.8026
Std. Dev.	608.01
Mean	13875.56
C.V. %	4.38
Significant	

3.9. Validation of Statistical Model.

The validation of the statistical model confirmed SF3 as the optimized batch. The experimental values for Spreadability and Viscosity with the predicted values by Design-Expert software, as shown in Table 9, indicate the

model high accuracy. The minimal standard deviation in Viscosity reinforces the reliability of the formulation process, establishing SF3 as the batch that meets the optimization criteria set by the study. The SF3 batch indicated as an optimized batch proved that the model was successfully validated.

Table 9: The predicted and experimental values of response variables and percentage error.

F.	Composition	Response	Predicted	Experimental	Percentage Error
----	-------------	----------	-----------	--------------	------------------

Code	(%w/v)		value	value	
SF3	Carbopol 934	Spreadability	13.7	13.6	-0.1
	PEG 400				
SF3	Carbopol 934	Viscosity	18108	17727	-381
	PEG 400				

3.10. Results of *In-vitro* drug release

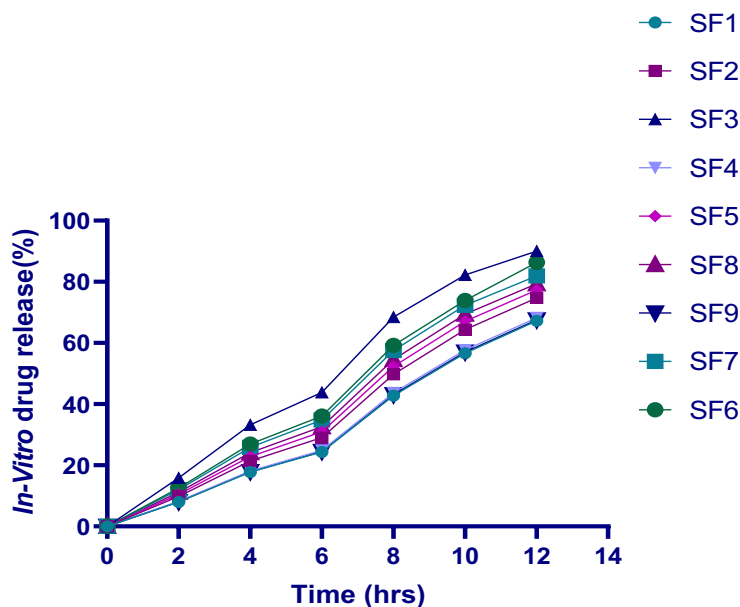


Figure 9: *In-Vitro* drug release studies of SF1 to SF9

The *in-vitro* drug release profiles of the MSPs loaded nanogel formulations (SF1 to SF9) over a 12-hour period are depicted in Figure 9. The data illustrates the cumulative percentage of drug released at specific time intervals, highlighting the release kinetics for each formulation. Initially, at the 2-hour mark, SF3 demonstrates the highest drug release (15.89%), followed by SF6 (12.57%) and SF7 (12.04%), indicating a faster initial release compared to the other formulations. This trend continues throughout the study, with SF3 consistently showing superior drug release rates, reaching 90.04% at the 12-hour mark. In contrast, formulations such as SF1 and SF9 exhibit slower release profiles, with SF1 reaching 67.2% and SF9 reaching 67.57% by the end of the 12-hour period. The variation in drug release rates among the formulations can be attributed to differences in

the concentrations of Carbopol® 934P and PEG 400, as these excipients significantly influence the release characteristics. SF3, with the highest release rate, likely contains an optimal balance of these components, enhancing the diffusion of the drug from the gel matrix. Conversely, the slower release observed in SF1 and SF9 suggests a higher viscosity or stronger gel network, which could retard drug diffusion. The intermediate release profiles of other formulations, such as SF4, SF5, and SF8, indicate varying degrees of drug diffusion control, potentially offering tailored release profiles for specific therapeutic requirements. Overall, the *in-vitro* release data provides critical insights for selecting the optimal formulation based on the desired release kinetics for effective drug delivery.

3.11. Results Stability study

Table 10: Result of stability study on various parameters of optimized batch (SF3) of RA-MSPs loaded gel. ($40 \pm 2^\circ\text{C}$ temperature and $75 \pm 5\%$ RM).

Response	Months			
	0	1	2	3
Appearance	Clear, Thick	Clear, Thick	Clear, Thick	Clear, Thick

Odor	Odourless	Odourless	Odourless	Odourless
Viscosity (cps)	17653±43.43	17663±42.45	17638±51.76	17638±40.44
pH	6.7±0.07	6.7±0.03	6.6±0.09	6.6±0.08
Spreadability (cm)	13.7±0.71	13.4±0.78	13.8±0.43	13.9±0.74

The stability study of the RA-MSPs loaded gel as provided in Table 10, conducted over a period of three months at 40±2°C and 75±5% relative humidity, demonstrates remarkable consistency in various physical and chemical parameters. Throughout the study period, the appearance of the gel remained clear and thick, indicating no visible signs of degradation or phase separation. The odour also remained consistently odourless, suggesting the absence of any volatile degradation products that could affect the formulation's stability. These observations suggest that the RA-MSPs loaded gel maintains its physical integrity and aesthetic appeal under accelerated stability conditions. In terms of quantitative measures, the viscosity of the gel showed minimal variation, with values ranging from 17638±40.44 cps to 17663±42.45 cps, indicating stable rheological properties over the three-month period. The pH values exhibited only slight fluctuations, from 6.7±0.07 at the beginning to 6.6±0.08 at the end, remaining within the acceptable range for topical formulations, which is crucial for maintaining skin compatibility and minimizing irritation. Spreadability values also remained stable, with a minor increase from 13.7±0.71 cm to 13.9±0.74 cm, indicating consistent ease of application. These results collectively demonstrate that the RA-MSPs loaded gel is stable under accelerated conditions, maintaining its physical properties, pH, viscosity, and spreadability, thereby ensuring its efficacy and usability over time.

4. CONCLUSION

The comprehensive evaluation of the RA-MSPs loaded nanogel formulations demonstrates their potential as an effective and stable topical delivery system for *Ruallia Asperula* extract. The calibration curve confirms the reliability of the quantitative analysis method, while the solubility studies identify ethanol as the optimal solvent for the extract. FTIR and DSC analyses reveal minor interactions between the extract and excipients, ensuring the chemical integrity and thermal stability of the formulation. The high entrapment efficiency and appropriate nanoscale particle size further validate the suitability of MSPs as a delivery vehicle. The physical characteristics, pH, spreadability, and viscosity of the formulations remained consistent, indicating a robust manufacturing process. The in-vitro drug release studies highlight the formulation's ability to provide sustained drug release, with SF3 emerging as the optimized batch. Stability studies confirm the long-term physical and chemical stability of the RA-MSPs loaded gel under accelerated conditions. Overall, these findings underscore the efficacy and stability of the RA-MSPs loaded nanogel, making it a promising candidate for wound healing applications.

ABBREVIATIONS

ANOVA: Anova of Variance; FTIR: Fourier-transform infrared spectroscopy; DSC: Differential scanning

calorimetry; UV: Ultra-violet spectroscopy; Df: Degree of freedom; RA: *Ruallia Asperula*; MSPs: Mesoporous silica Particles.

ACKNOWLEDGEMENT

The authors sincerely acknowledge the constant support and valuable guidance of Dr. Sachin N. Kothawade, Principal, Sitabai Thite College of Pharmacy, Shirur, during the course of this research. His encouragement and constructive suggestions were instrumental in the successful completion of this study. The authors are also grateful to Sciquaint Innovations (OPC) Private Limited, Pune, India, for kindly providing the *Ruallia asperula* extract used in this investigation.

CONSENT TO PARTICIPATE

All authors confirm their consent to actively participate in this research work.

CONSENT TO PUBLISH

All authors have reviewed and approved the final version of the manuscript for publication. The manuscript is original, has not been published elsewhere, and is not under consideration in any other journal.

DISCLOSURE STATEMENT

The authors declare that there are no conflicts of interest regarding this work.

DATA AVAILABILITY STATEMENT

All relevant data generated and analyzed during this study are included in this article. Additional datasets can be made available from the corresponding author upon reasonable request.

FUNDING

This research was carried out without any external funding.

REFERENCES

- [1] L. Cañedo-Dorantes and M. Cañedo-Ayala, "Skin Acute Wound Healing: A Comprehensive Review," *Int. J. Inflamm.*, vol. 2019, p. e3706315, Jun. 2019, doi: 10.1155/2019/3706315.
- [2] C. Politis, J. Schoenaers, R. Jacobs, and J. O. Agbaje, "Wound Healing Problems in the Mouth," *Front. Physiol.*, vol. 7, Nov. 2016, doi: 10.3389/fphys.2016.00507.
- [3] A. Ridiandries, J. T. M. Tan, and C. A. Bursill, "The Role of Chemokines in Wound Healing," *Int. J. Mol. Sci.*, vol. 19, no. 10, Art. no. 10, Oct. 2018, doi: 10.3390/ijms19103217.
- [4] M. Abazari, A. Ghaffari, H. Rashidzadeh, S. M. Badeleh, and Y. Maleki, "A Systematic Review on Classification, Identification, and Healing Process of Burn Wound Healing," *Int. J. Low. Extrem. Wounds*, vol. 21, no. 1, pp. 18–30, Mar. 2022, doi: 10.1177/1534734620924857.

- [5] A. C. de O. Gonzalez, T. F. Costa, Z. de A. Andrade, and A. R. A. P. Medrado, "Wound healing - A literature review," *An. Bras. Dermatol.*, vol. 91, pp. 614–620, Oct. 2016, doi: 10.1590/abd1806-4841.20164741.
- [6] A. A. Vasconcelos *et al.*, "Chemical composition determination and evaluation of the antibacterial activity of essential oils from *Ruellia asperula* (Mart. Ex Ness) Lindau and *Ruellia paniculata* L. against oral streptococci," *Nat. Prod. Res.*, vol. 37, no. 2, pp. 333–337, Jan. 2023, doi: 10.1080/14786419.2021.1960521.
- [7] K. Afzal, M. Uzair, B. A. Chaudhary, A. Ahmad, S. Afzal, and M. Saadullah, "GENUS RUELLIA: PHARMACOLOGICAL AND PHYTOCHEMICAL IMPORTANCE IN ETHNOPHARMACOLOGY".
- [8] B. Korica, "Asperula visianii, nova spec., und A. staliana (Rubiaceae), Endemiten der Inseln Mitteldalmatiens," *Plant Syst. Evol.*, vol. 133, no. 1, pp. 71–76, Mar. 1979, doi: 10.1007/BF00985880.
- [9] E. Tenland *et al.*, "Effective delivery of the antimycobacterial peptide NZX in mesoporous silica nanoparticles," *PLOS ONE*, vol. 14, no. 2, p. e0212858, Feb. 2019, doi: 10.1371/journal.pone.0212858.
- [10] A. Bernardos *et al.*, "Mesoporous Silica-Based Materials with Bactericidal Properties," *Small*, vol. 15, no. 24, p. 1900669, 2019, doi: 10.1002/sml.201900669.
- [11] R. Narayan, U. Y. Nayak, A. M. Raichur, and S. Garg, "Mesoporous Silica Nanoparticles: A Comprehensive Review on Synthesis and Recent Advances," *Pharmaceutics*, vol. 10, no. 3, Art. no. 3, Sep. 2018, doi: 10.3390/pharmaceutics10030118.
- [12] N. I. Vazquez, Z. Gonzalez, B. Ferrari, and Y. Castro, "Synthesis of mesoporous silica nanoparticles by sol-gel as nanocontainer for future drug delivery applications," *Bol. Soc. Esp. Cerámica Vidr.*, vol. 56, no. 3, pp. 139–145, May 2017, doi: 10.1016/j.bsecv.2017.03.002.
- [13] S. Jafari, H. Derakhshankhah, L. Alaei, A. Fattahi, B. S. Varnamkhasti, and A. A. Saboury, "Mesoporous silica nanoparticles for therapeutic/diagnostic applications," *Biomed. Pharmacother.*, vol. 109, pp. 1100–1111, Jan. 2019, doi: 10.1016/j.biopha.2018.10.167.
- [14] J. Florek, R. Caillard, and F. Kleitz, "Evaluation of mesoporous silica nanoparticles for oral drug delivery – current status and perspective of MSNs drug carriers," *Nanoscale*, vol. 9, no. 40, pp. 15252–15277, Oct. 2017, doi: 10.1039/C7NR05762H.
- [15] Q. Zheng, S. Li, X. Li, and R. Liu, "Advances in the study of emodin: an update on pharmacological properties and mechanistic basis," *Chin. Med.*, vol. 16, no. 1, p. 102, Oct. 2021, doi: 10.1186/s13020-021-00509-z.
- [16] S. El-Housiny *et al.*, "Fluconazole-loaded solid lipid nanoparticles topical gel for treatment of pityriasis versicolor: formulation and clinical study," *Drug Deliv.*, vol. 25, no. 1, pp. 78–90, Jan. 2018, doi: 10.1080/10717544.2017.1413444.
- [17] H. N. Ho *et al.*, "Development of Itraconazole-Loaded Polymeric Nanoparticle Dermal Gel for Enhanced Antifungal Efficacy," *J. Nanomater.*, vol. 2020, p. e8894541, Dec. 2020, doi: 10.1155/2020/8894541.
- [18] N. A. H. A. Youssef, A. A. Kassem, R. M. Farid, F. A. Ismail, M. A. E. EL-Massik, and N. A. Boraie, "A novel nasal almotriptan loaded solid lipid nanoparticles in mucoadhesive *in situ* gel formulation for brain targeting: Preparation, characterization and *in vivo* evaluation," *Int. J. Pharm.*, vol. 548, no. 1, pp. 609–624, Sep. 2018, doi: 10.1016/j.ijpharm.2018.07.014.
- [19] S. M. Mirsalami and M. Mirsalami, "Evaluation of mesoporous silica particles as a support for lipase immobilization in biodiesel production: Enhanced ethyl ester synthesis from algal oil," *Results Eng.*, vol. 22, p. 102138, Jun. 2024, doi: 10.1016/j.rineng.2024.102138.
- [20] S. Rajput, N. Vadia, and M. Mahajan, "Role of Mesoporous Silica Nanoparticles as Drug Carriers: Evaluation of Diverse Mesoporous Material Nanoparticles as Potential Host for Various Applications," in *Advanced Functional Porous Materials: From Macro to Nano Scale Lengths*, A. Uthaman, S. Thomas, T. Li, and H. Maria, Eds., Cham: Springer International Publishing, 2022, pp. 205–234. doi: 10.1007/978-3-030-85397-6_7.
- [21] S. N. Shrotriya, B. V. Vidhate, and M. S. Shukla, "Formulation and development of Silybin loaded solid lipid nanoparticle enriched gel for irritant contact dermatitis," *J. Drug Deliv. Sci. Technol.*, vol. 41, pp. 164–173, Oct. 2017, doi: 10.1016/j.jddst.2017.07.006.
- [22] G. Shilakari Asthana, A. Asthana, D. Singh, and P. K. Sharma, "Etodolac Containing Topical Niosomal Gel: Formulation Development and Evaluation," *J. Drug Deliv.*, vol. 2016, no. 1, p. 9324567, 2016, doi: 10.1155/2016/9324567.
- [23] M. Qushawy, A. Nasr, M. Abd-Alhaseeb, and S. Swidan, "Design, Optimization and Characterization of a Transfersomal Gel Using Miconazole Nitrate for the Treatment of Candida Skin Infections," *Pharmaceutics*, vol. 10, no. 1, Art. no. 1, Mar. 2018, doi: 10.3390/pharmaceutics10010026.
- [24] I. Akbarzadeh *et al.*, "Optimization, physicochemical characterization, and antimicrobial activity of a novel simvastatin nano-niosomal gel against *E. coli* and *S.*

aureus,” *Chem. Phys. Lipids*, vol. 234, p. 105019, Jan. 2021, doi: 10.1016/j.chemphyslip.2020.105019.